Electronic Supplementary Material (ESI) for Materials Chemistry Frontiers.
This journal is © the Partner Organisations 2021

Supplementary Information for

Dinuclear Anthracene-Containing Alkynylplatinum(II) Terpyridine Complexes with Photo-Modulated Self-Assembly Behaviors

Shishi Fang, Michael Ho-Yeung Chan, and Vivian Wing-Wah Yam*

Institute of Molecular Functional Materials and Department of Chemistry, The University of Hong Kong, Pokfulam Road, Hong Kong (P. R. China)

E-mail: wwyam@hku.hk; Fax: (852) 28571586; Tel: (852) 28592153

Experimental Section

Materials and Reagents. Potassium tetrachloroplatinate(II) ($K_2[PtCl_4]$) was purchased from Chem. Pur., 98%. Dimethyl sulfoxide (Sigma-Aldrich Co. Ltd., spectrophotometric grade) for spectroscopic studies were used as received without further purification. Chloroform-*d* and DMSO-d_6 used for NMR experiments were purchased from Cambridge Isotope Laboratories, Inc. All other reagents, unless otherwise specified, were of analytical grade and were used as received. 9,10-Diethynylanthracene[1] and [Pt{tpy–C_6H_3–$(alkoxy)_2$-3,5}Cl]OTf[2] were prepared according to previously reported literature with slight modifications.

Synthesis of Dinuclear Anthracene-Containing Alkynylplatinum(II) Terpyridine Complexes 1–3. The dinuclear anthracene-containing alkynylplatinum(II) terpyridine complexes were synthesized according to modifications of procedures for the synthesis of dinuclear alkynylplatinum(II) terpyridine derivatives previously reported by Yam and coworkers in the literature.[3]

[{tpy–C_6H_3–$(OTEG)_2$-3,5}Pt{C≡C–(9-Ant)–C≡C}Pt{tpy–Ph–$(OTEG)_2$-3,5}]$(OTf)_2$ (1). To a solution of 9,10-diethynylanthracene (14 mg, 0.06 mmol) and [Pt{tpy–C_6H_3–$(OTEG)_2$-3,5}Cl]OTf (132 mg, 0.13 mmol) in degassed dimethylformamide (30 ml) containing triethylamine (2 ml) was added a catalytic amount of CuI. The solution was stirred at room temperature in the dark under a nitrogen atmosphere overnight. After removing the solvent, the crude product was purified by the diffusion of diethyl ether vapor into a dichloromethane-chloroform mixture to give a dark green solid. Yield: 67 mg (51 %). ^{1}H NMR (500 MHz, DMSO-d_6, 373 K): δ/ppm = 3.27 (s, 12H, –OCH_3), 3.49 (s, 8H, –OCH_2–), 3.59–3.66 (m, 24H, –OCH_2–), 3.78 (s, 8H, –OCH_2–), 4.11 (s, 8H, –OCH_2–), 6.59 (s, 2H, –C_6H_3–), 7.30–7.35 (m, 8H,

–C_6H_3– and –$C_{14}H_8$–), 7.98 (s, 4H, tpy), 8.48–8.53 (m, 8H, tpy), 8.79 (s, 4H, tpy), 8.90 (s, 4H, –$C_{14}H_8$–), 9.10 (s, 4H, tpy). Positive HR-ESI-MS: calcd for $[C_{88}H_{94}N_6O_{16}Pt_2]^{2+}$ *m/z* = 940.3011; found: 940.2981 $[M]^{2+}$; elemental analysis calcd (%) for $C_{90}H_{94}F_6N_6O_{22}Pt_2S_2 \bullet CH_2Cl_2$: C 48.26, H 4.27, N 3.71; found: C 48.20, H 4.37, N 3.85.

[{tpy–C_6H_3–$(OC_{12}H_{25})_2$-3,5}Pt{C≡C–(9-Ant)–C≡C}Pt{tpy–Ph–$(OC_{12}H_{25})_2$-3,5}]$(OTf)_2$ (2). The titled complex was synthesized according to the procedure similar to that described for the preparation of **1**, except that [Pt{tpy–C_6H_3–$(OC_{12}H_{25})_2$-3,5}Cl]OTf (137 mg, 0.13 mmol) was used in place of [Pt{tpy–C_6H_3–$(OTEG)_2$-3,5}Cl]OTf. The product was isolated as a dark green solid. Yield: 71 mg (52 %). ^{1}H NMR (500 MHz, DMSO-d_6, 373 K): δ/ppm = 0.88 (s, 12H, –CH_3), 1.29–1.42 (m, 72H, –CH_2–), 1.70 (s, 8H, –CH_2–), 3.92 (s, 8H, –OCH_2–), 6.46 (s, 2H, –C_6H_3–), 7.22–7.29 (m, 8H, –C_6H_3– and –$C_{14}H_8$–), 7.96 (s, 4H, tpy), 8.39 (s, 4H, tpy), 8.50 (s, 4H, tpy), 8.79 (d, *J* = 5.5 Hz, 4H, tpy), 8.87 (s, 4H, –$C_{14}H_8$–), 9.03 (s, 4H, tpy). Positive HR-ESI-MS: calcd for $[C_{108}H_{134}N_6O_4Pt_2]^{2+}$ *m/z* = 984.4881; found: 984.4915 $[M]^{2+}$; elemental analysis calcd (%) for $C_{110}H_{134}F_6N_6O_{10}Pt_2S_2 \bullet CHCl_3$: C 55.83, H 5.70, N 3.52; found: C 55.64, H 5.75, N 3.59.

[{tpy–C_6H_3–$(OC_{18}H_{37})_2$-3,5}Pt{C≡C–(9-Ant)–C≡C}Pt{tpy–Ph–$(OC_{18}H_{37})_2$-3,5}]$(OTf)_2$ (3). The titled complex was synthesized according to the procedure similar to that described for the preparation of **1**, except that [Pt{tpy–C_6H_3–$(OC_{18}H_{37})_2$-3,5}Cl]-OTf (159 mg, 0.13 mmol) was used in place of [Pt{tpy–C_6H_3–$(OTEG)_2$-3,5}Cl]OTf. The product was isolated as a dark green solid. Yield: 80 mg (51 %). ^{1}H NMR (500 MHz, DMSO-d_6, 373 K): δ/ppm = 0.86 (t, *J* = 7.0 Hz, 12H, –CH_3), 1.26–1.39 (m, 112H, –CH_2–), 1.43–1.48 (m, 8H, –CH_2–), 1.72–1.76 (m, 8H, –CH_2–), 4.02 (s, 8H, –OCH_2–), 6.58 (s, 2H, –C_6H_3–), 7.28 (s, 4H, –$C_{14}H_8$–), 7.45 (s, 4H, –C_6H_3–), 7.99 (t, *J* = 7.0 Hz, 4H, tpy), 8.53–8.60 (m, 8H, tpy), 8.86 (d, *J* = 8.0 Hz, 4H, tpy), 8.94 (s, 4H, –$C_{14}H_8$–), 9.19 (s, 4H, tpy). Positive HR-ESI-MS: calcd for $[C_{132}H_{182}N_6O_4Pt_2]^{2+}$ *m/z* = 1152.6759;

found: 1152.6737 $[M]^{2+}$; elemental analysis calcd (%) for $C_{134}H_{182}F_6N_6O_{10}Pt_2S_2 \bullet 0.5CH_2Cl_2$: C 61.01, H 6.97, N 3.17; found: C 60.91, H 7.01, N 3.26.

Photophysical Measurements and Instrumentation. ^{1}H NMR spectra were recorded on a Bruker Ascend 500 (500 MHz) Fourier-transform NMR spectrometer with chemical shifts reported relative to tetramethylsilane, $(CH_3)_4Si$. Positive-ion high-resolution electrospray ionization (HR-ESI) mass spectra were recorded on a Bruker maXis II High Resolution Liquid Chromatography Quadrupole-Time of Flight (LC-QTOF) spectrometer. Elemental analyses were performed with a Carlo Erba 1106 elemental analyzer at the Institute of Chemistry, Chinese Academy of Sciences, Beijing, P. R. China. UV–Vis absorption spectra for variable concentration and temperature measurements were recorded using a Varian Cary 50 UV–vis spectrophotometer. The temperature was maintained by a Varian Cary single cell Peltier thermostat. UV–Vis absorption spectral changes during photoirradiation were recorded on a Cary 8454 spectrophotometer. Photoirradiations were carried out with a 300 W Oriel Corporation Model 60011 Xe (ozone-free) lamp with an Applied Photophysics F 3.4 monochromator to select the monochromatic light. Transmission electron microscopy (TEM) experiments were performed on a Philips CM100 TEM equipped with a TENGRA 2.3 K × 2.3 K camera for digital imaging, while the selected area electron diffraction (SAED) experiments were performed on a FEI Tecnai G2 20 S-TWIN transmission electron microscope with an accelerating voltage of 200 kV. Scanning electron microscopy (SEM) experiments were performed on a Hitachi S4800 FEG SEM. Dynamic light scattering (DLS) was measured with a Malvern Zetasizer Nano ZS90 equipped with an internal HeNe laser (633.0 nm) at different temperatures. All measurements were conducted at room temperature unless specified otherwise.

Isodesmic Model in Curve Fitting. The isodesmic model[4] developed by Meijer and coworkers has been applied to fit the melting curves obtained in the temperature-dependent UV–vis spectroscopic studies for complexes **1**–**3** in DMSO solutions. A slow cooling rate of 0.5 K min^{-1} was applied for all melting curves to ensure that the self-assembly processes were under thermodynamic control.[5−7] The self-assembly process can be described as isodesmic growth mechanism if every monomer addition to the supramolecular polymer is governed by a single equilibrium constant K_e. In the isodesmic model, the degree of aggregation (α) is related to the absolute temperature T by equation (1) as shown below. The melting temperature T_m is defined as the temperature when α = 0.5, while the enthalpy change ΔH corresponds to the formation of non-covalent interactions during the aggregation process. R is the ideal gas constant.

$$\alpha(T) = \frac{1}{1 + \exp\left[-0.908\Delta H \frac{T - T_m}{RT_m^2}\right]} \qquad \text{eqn. (1)}$$

The equation above could be applied to fit the experimental data of UV–vis absorption spectra at various temperatures so that the ΔH and T_m could be obtained. In addition, the average stack length DP_N and the equilibrium constant K_e can be obtained by equation (2) with known concentration c.

$$DP_N = \frac{1}{\sqrt{1 - \alpha(T)}} = \frac{1}{2} + \frac{1}{2}\sqrt{4K_e(T)c + 1} \qquad \text{eqn. (2)}$$

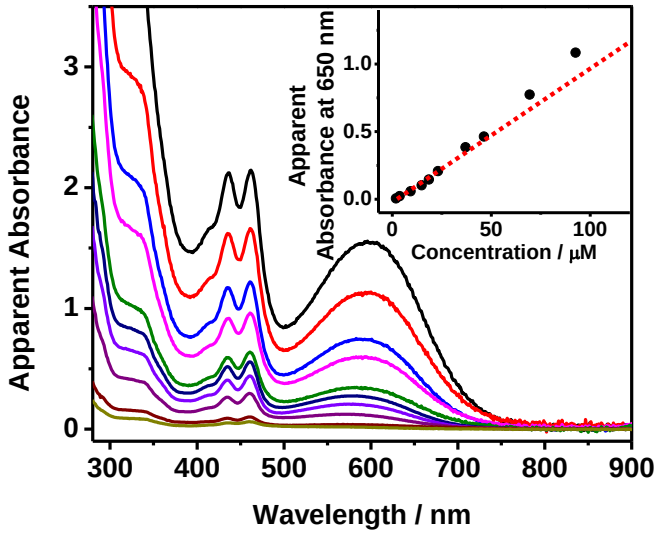

Figure S1. Concentration-dependent UV–vis absorption spectra of complex **2** in DMSO solution in the concentration range of 1.85×10^{-6} to 9.26×10^{-5} M. Inset: A plot of apparent absorbance against concentration, monitored at 650 nm. The apparent absorbance values were obtained by correcting to 1-cm path length equivalence.

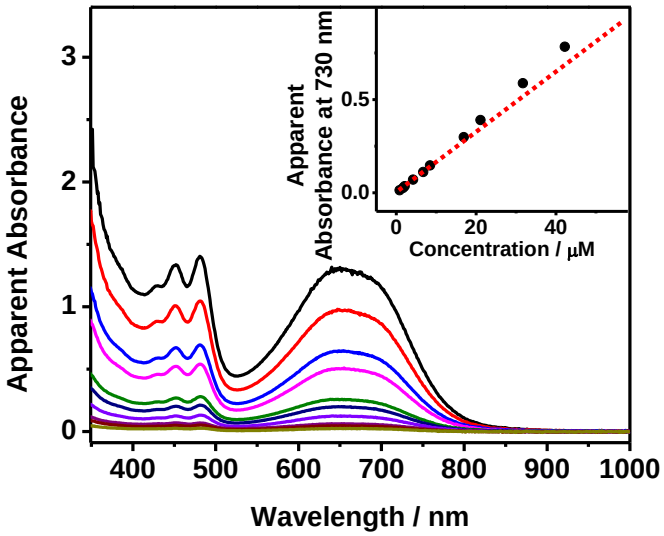

Figure S2. Concentration-dependent UV–vis absorption spectra of complex **3** in DMSO solution in the concentration range of 8.44×10^{-7} to 4.22×10^{-5} M. Inset: A plot of apparent absorbance against concentration, monitored at 730 nm. The apparent absorbance values were obtained by correcting to 1-cm path length equivalence.

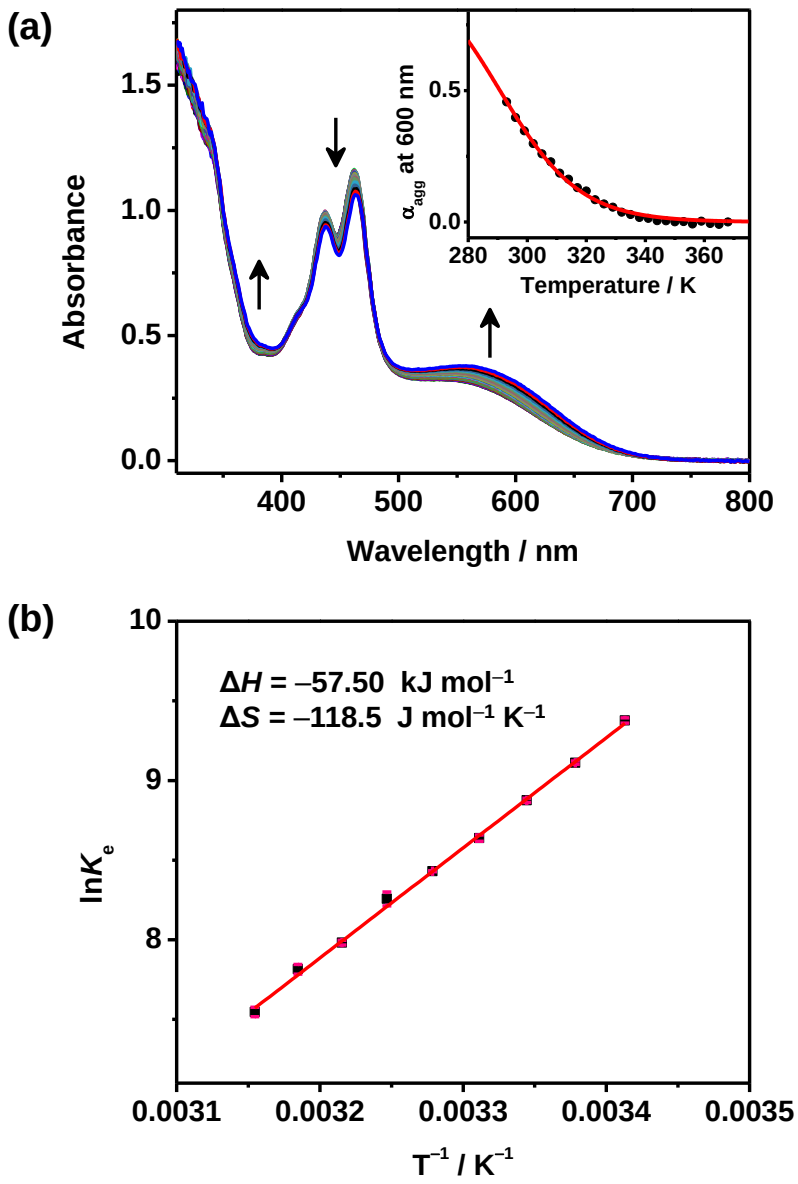

Figure S3. (a) UV–Vis absorption spectral traces of complex **1** in DMSO solution upon cooling from 368 to 293 K at a rate of 0.5 K min^{-1}. Inset: A plot of the degree of aggregation at 600 nm as a function of temperature with the curve fitted to the temperature-dependent isodesmic model. (b) Van't Hoff plot of the equilibrium constant K_e at various temperatures with the corresponding thermodynamic parameters.

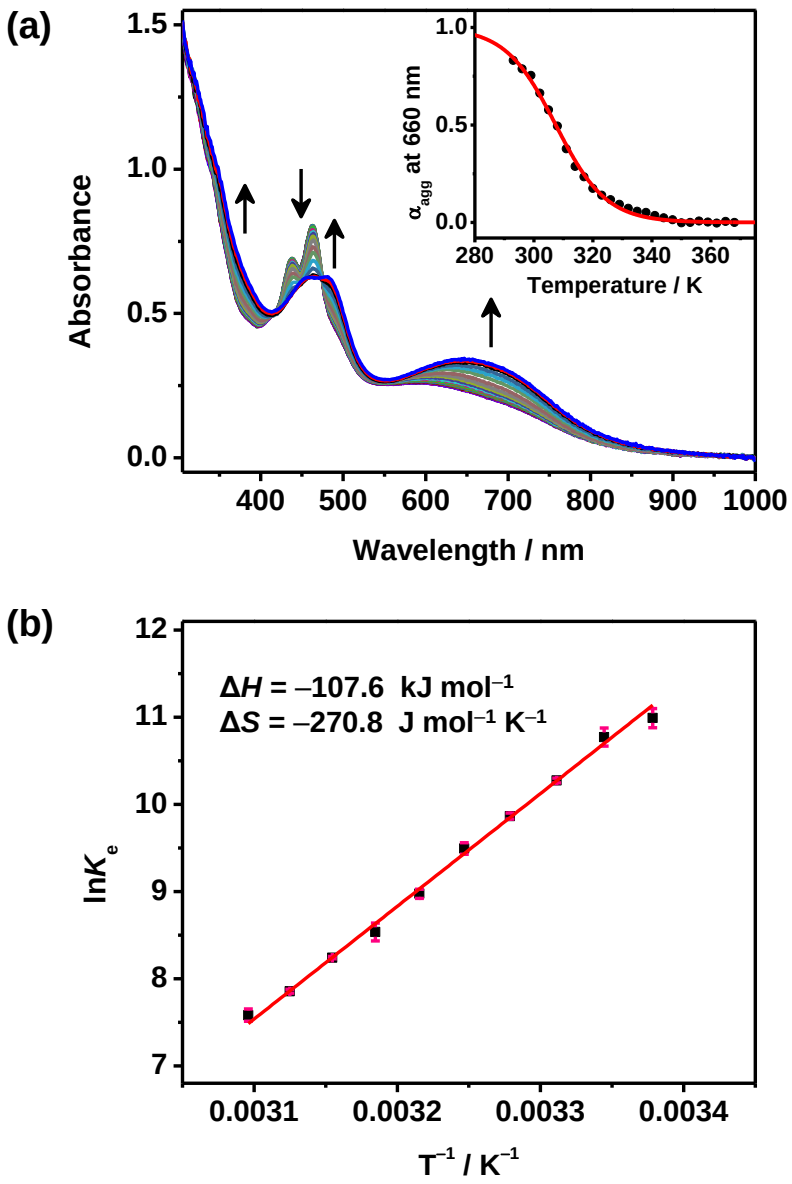

Figure S4. (a) UV–Vis absorption spectral traces of complex **3** in DMSO solution upon cooling from 368 to 293 K at a rate of 0.5 K min^{-1}. Inset: A plot of the degree of aggregation at 660 nm as a function of temperature with the curve fitted to the temperature-dependent isodesmic model. (b) Van't Hoff plot of the equilibrium constant K_e at various temperatures with the corresponding thermodynamic parameters.

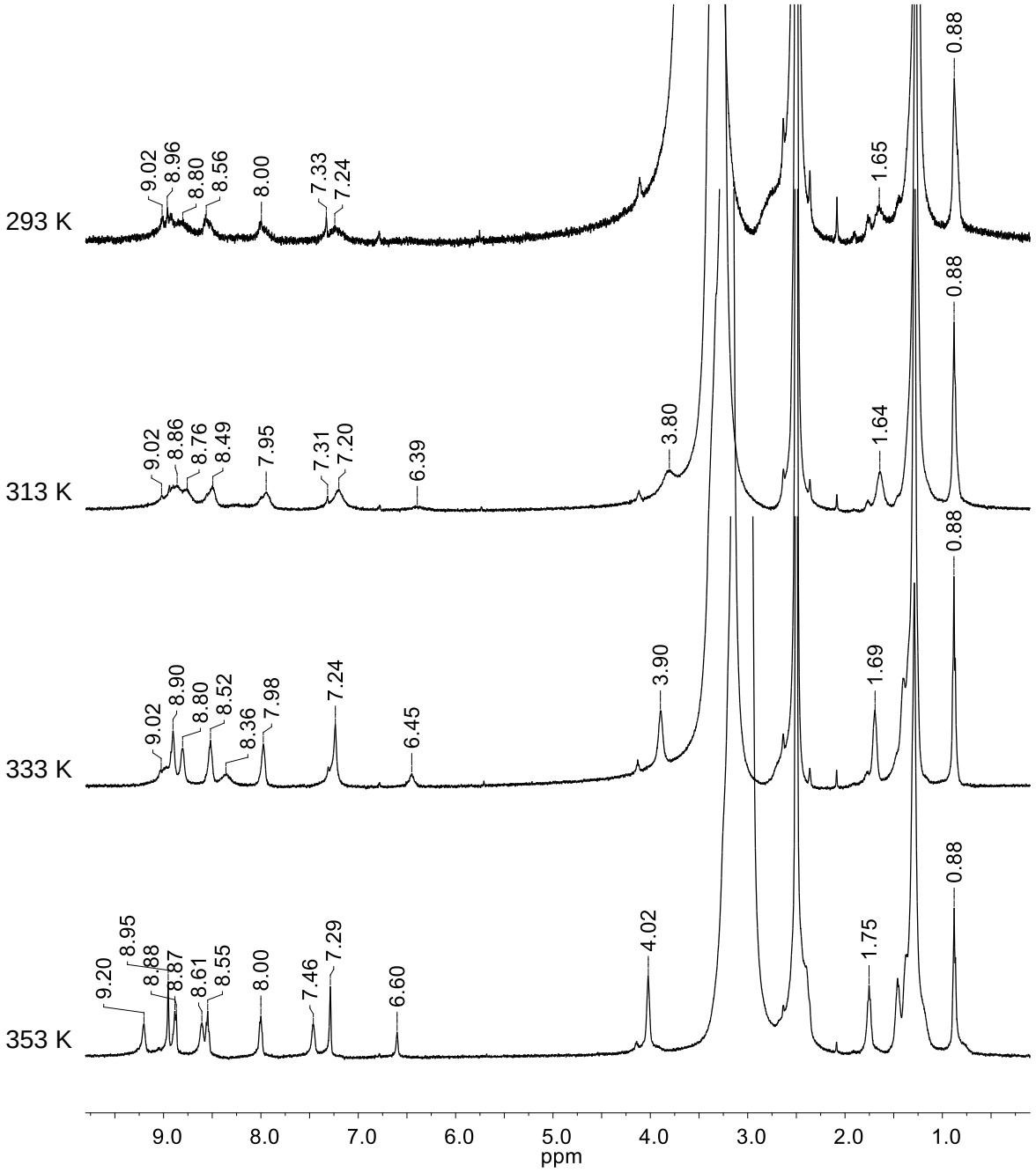

Figure S5. ^{1}H NMR spectra of complex **2** in DMSO-d_6 solution upon increasing temperature from 293 K to 353 K.

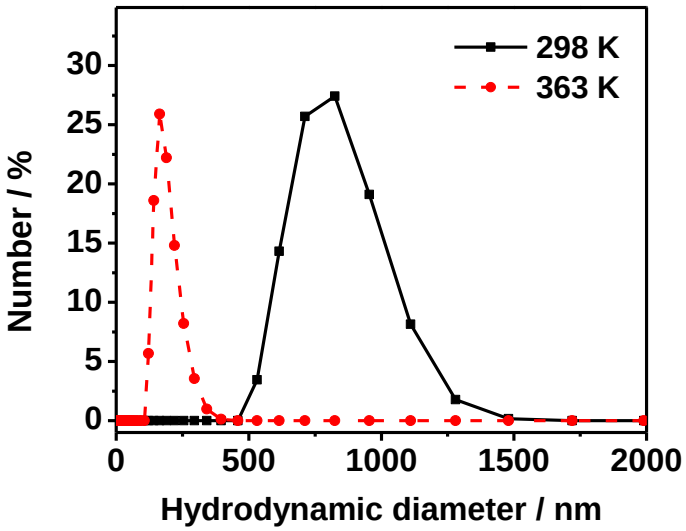

Figure S6. DLS data of complex **3** in DMSO solution at 298 K and 363 K, with the hydrodynamic diameters of *ca*. 860 nm and 210 nm, respectively.

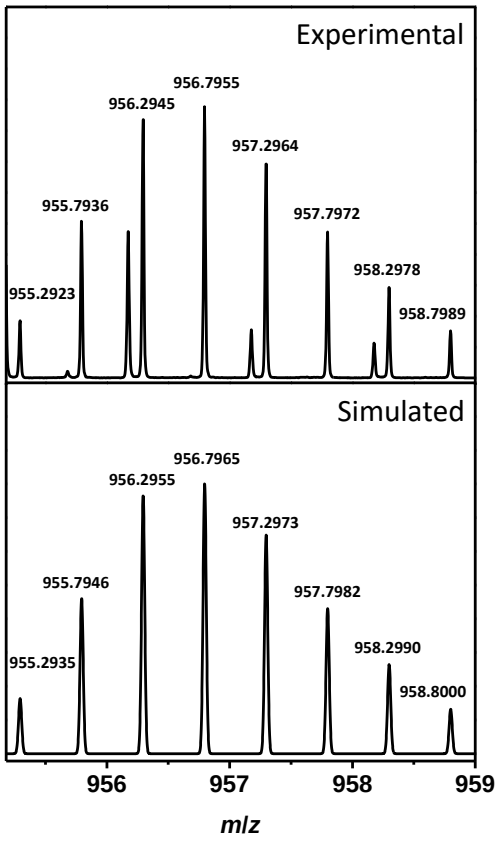

Figure S7. HR-ESI-MS showing the corresponding endoperoxide $[M+2O]^{2+}$ of complex **1** after photoirradiation and the corresponding simulated isotopic pattern.

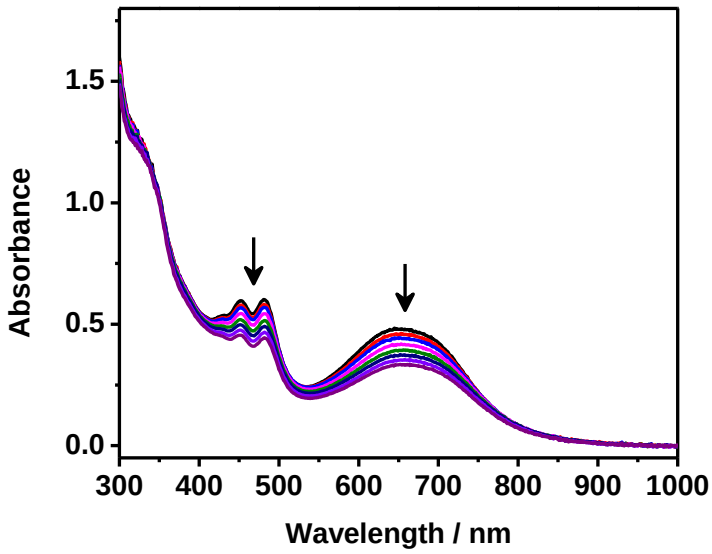

Figure S8. UV–Vis absorption spectral changes of complex **3** in DMSO solution upon photoirradiation at 365 nm at 298 K.

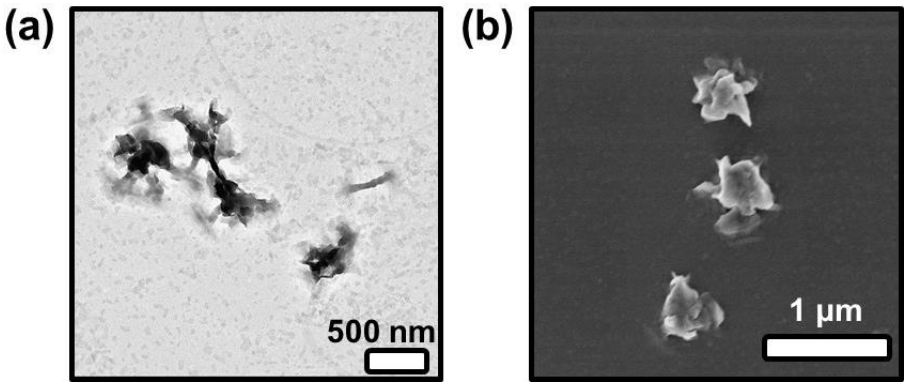

Figure S9. (a) A TEM image and (b) an SEM image of complex **3** prepared from a DMSO solution after photoirradiation.

Table S1. Electronic absorption data of complexes **1**–**3** in DMSO solutions

Complex	Temperature / K	Absorption λ_{max} / nm (ε / dm^3 mol^{-1} cm^{-1})
[{tpy–C_6H_3–$(OTEG)_2$-3,5}Pt–{C≡C–(9-Ant)–C≡C}Pt{tpy–C_6H_3–$(OTEG)_2$-3,5}]$(OTf)_2$ (**1**)	298	315sh (43200), 335sh (39600), 413sh (18700), 434sh (28800), 460sh (32400), 568 (12000)
	368	314sh (41400), 339sh (36500), 413sh (18300), 434sh (30900), 460sh (37300), 549 (9640)
[{tpy–C_6H_3–$(OC_{12}H_{25})_2$-3,5}Pt–{C≡C–(9-Ant)–C≡C}Pt{tpy–C_6H_3–$(OC_{12}H_{25})_2$-3,5}]$(OTf)_2$ (**2**)	298	312sh (38100), 414sh (16100), 435sh (22100), 461sh (23300), 590 (13200)
	368	312sh (37900), 337sh (31400), 414sh (16600), 435sh (28500), 460sh (34100), 553 (8520)
[{tpy–C_6H_3–$(OC_{18}H_{37})_2$-3,5}Pt–{C≡C–(9-Ant)–C≡C}Pt{tpy–C_6H_3–$(OC_{18}H_{37})_2$-3,5}]$(OTf)_2$ (**3**)	298	313sh (27300), 433sh (11000), 453sh (12200), 481sh (12000), 639sh (11300), 682sh (10400)
	368	313sh (27100), 337sh (24800), 411sh (12300), 435sh (21200), 460sh (25000), 558sh (8150)

Table S2. Thermodynamic parameters for the self-assembly of complexes **1**–**3** in DMSO solutions

Complex	ΔH / kJ mol^{-1}	T_m[a] / K	K_e[a] / M^{-1}	ΔS[b] / J mol^{-1} K^{-1}	ΔG[b] / kJ mol^{-1}	DP_N
[{tpy–C_6H_3–$(OTEG)_2$-3,5}Pt{C≡C–(9-Ant)–C≡C}Pt{tpy–C_6H_3–$(OTEG)_2$-3,5}]$(OTf)_2$ (**1**)	–57.28[a] –57.50[b]	291	9.06×10^3	–118.5	–22.2	1.3
[{tpy–C_6H_3–$(OC_{12}H_{25})_2$-3,5}Pt{C≡C–(9-Ant)–C≡C}Pt{tpy–C_6H_3–$(OC_{12}H_{25})_2$-3,5}]$(OTf)_2$ (**2**)	–77.72[a] –75.86[b]	305	3.49×10^4	–169.0	–25.5	1.8
[{tpy–C_6H_3–$(OC_{18}H_{37})_2$-3,5}Pt{C≡C–(9-Ant)–C≡C}Pt{tpy–C_6H_3–$(OC_{18}H_{37})_2$-3,5}]$(OTf)_2$ (**3**)	–101.2[a] –107.6[b]	307	5.93×10^4	–270.8	–26.9	2.2

[a] Determined by fitting the experimental data of the functions of normalized degree of aggregation against temperature on the basis of the temperature-dependent isodesmic model.

[b] Determined by the van't Hoff plot generated from the variable-temperature UV–vis absorption studies.

Table S3. DLS data of complex **3** in DMSO solution before and after photoirradiation at room temperature

Sample condition	Hydrodynamic diameter / nm
Before photoirradiation	863.7 ± 162.7
After photoirradiation	776.2 ± 171.2

References

1 S. Yu, R. Shan, G.-Y. Sun, T. Chen, L. Wu and L. Y. Jin, Construction of various supramolecular assemblies from rod−coil molecules containing biphenyl and anthracene groups driven by donor−acceptor iInteractions, *ACS Appl. Mater. Interfaces*, 2018, **10**, 22529–22536.

2 V. W.-W. Yam, R. P.-L. Tang, K. M.-C. Wong and K.-K. Cheung, Synthesis, luminescence, electrochemistry, and ion-binding studies of platinum(II) terpyridyl acetylide complexes, *Organometallics*, 2001, **20**, 4476–4482.

3 K. H.-Y. Chan, H.-S. Chow, K. M.-C. Wong, M. C.-L. Yeung and V. W.-W. Yam, Towards thermochromic and thermoresponsive near-infrared (NIR) luminescent molecular materials through the modulation of inter- and/or intramolecular Pt···Pt and π–π interactions, *Chem. Sci.*, 2010, **1**, 477–482.

4 M. M. J. Smulders, M. M. L. Nieuwenhuizen, T. F. A. de Greef, P. van der Schoot, A. P. H. J. Schenning and E. W. Meijer, How to distinguish isodesmic from cooperative supramolecular polymerisation, *Chem.–Eur. J.*, 2010, **16**, 362–367.

5 P. Jonkheijm, P. van der Schoot, A. P. H. J. Schenning and E. W. Meijer, Probing the solvent-assisted nucleation pathway in chemical self-assembly, *Science*, 2006, **313**, 80–83.

6 M. M. J. Smulders, A. P. H. J. Schenning and E. W. Meijer, Insight into the mechanisms of cooperative self-assembly: the "sergeants-and-soldiers" principle of chiral and achiral C_3-symmetrical discotic triamides, *J. Am. Chem. Soc.*, 2008, **130**, 606–611.

7 P. A. Korevaar, C. Schaefer, T. F. A. de Greef and E. W. Meijer, Controlling chemical self-assembly by solvent-dependent dynamics, *J. Am. Chem. Soc.*, 2012, **134**, 13482–13491.